IOP PUBLISHING NANOTECHNOLOGY
Nanotechnology **18** (2007) 245605 (8pp) doi:10.1088/0957-4484/18/24/245605

Size and composition tunable Ag–Au alloy nanoparticles by replacement reactions

Qingbo Zhang[1], Jim Yang Lee[1], Jun Yang[1], Chris Boothroyd[2] and Jixuan Zhang[3]

[1] Department of Chemical and Biomolecular Engineering, National University of Singapore, 10 Kent Ridge Crescent, 119260, Singapore
[2] Institute of Materials Research and Engineering, Singapore 3 Research Link, 117602, Singapore
[3] Department of Material Science and Engineering, National University of Singapore, 10 Kent Ridge Crescent, 119260, Singapore

E-mail: cheleejy@nus.edu.sg

Received 15 March 2007, in final form 20 April 2007
Published 18 May 2007
Online at stacks.iop.org/Nano/18/245605

Abstract
Ag–Au alloy nanoparticles with tunable size and composition were prepared by a replacement reaction between Ag nanoparticles and $HAuCl_4$ at elevated temperatures. The formation of homogeneous alloy nanoparticles was confirmed by selected-area energy-dispersive x-ray spectroscopy (SAEDX), UV–visible absorption spectroscopy, high resolution transmission electron microscopy (HRTEM) and electron diffraction. This method leverages upon the rapid interdiffusion of Ag and Au atoms in the reduced dimension of a nanoparticle, elevated temperatures and the large number of vacancy defects created in the replacement reaction. This method of preparation has several notable advantages: (1) independent tuning of the size and composition of alloy nanoparticles; (2) production of alloy nanoparticles in high concentrations; (3) general utility in the synthesis of alloy nanoparticles that cannot be obtained by the co-reduction method.

1. Introduction

The properties of alloy nanoparticles can be very different from the properties of the component monometallic nanoparticles [1]. This provides yet another dimension in tailoring the properties of nanomaterials besides the usual size and shape manipulation. For example, Ag–Au alloy nanoparticles are more catalytically active than monometallic Ag or Au nanoparticles in the oxidation of CO at low temperatures, even though the monometallic nanoparticles are already an improvement over their bulk forms [2]. In addition, while monometallic Ag and Au nanoparticles have relatively unchanging optical properties due to surface plasmon response (SPR), the SPR properties of Ag–Au alloy nanoparticles are continuously tunable because of the possibility of composition changes [3].

Ag–Au alloy nanoparticles can be prepared by a number of methods, the most common one being the co-reduction of the corresponding metal precursor salts in the presence of a stabilizing agent [4–6]. Water-in-oil microemulsions have also been used by Chen to produce Ag–Au alloy nanoparticles [7]. In the digestive ripening method of Klabunde and coworkers [8], Ag–Au alloy nanoparticles were formed by refluxing Ag and Au nanoparticles in 4-tert-butyltoluene in the presence of an alkanethiol. Other methods of preparation of a more physical nature include laser ablation [9] and evaporation–condensation [10]. Despite a myriad of methods of preparation, the large-scale synthesis of alloy nanoparticles with good control of size and composition remains a challenge. First, size tuning by changing the synthesis conditions is more complex for the alloy nanoparticles than for the monometallic nanoparticles. This is because the synthesis conditions affect the reduction potentials and the effectiveness of the stabilizing agent in different ways. Second, most current methods of preparation are unable to decouple size and composition control, which increases the difficulty in producing alloy nanoparticles with the same composition but different sizes, or the same size with different compositions. In addition, Ag^+ has the propensity of forming insoluble halide precipitates whenever the synthesis

Table 1. Synthesis conditions for Ag nanoparticles with different sizes.

Ag nanoparticles	Volume of $AgNO_3$ (ml)	Volume of PVP (ml)	Volume of KOH (ml)	Volume of $NaBH_4$ (ml)	Volume of H_2O (ml)
Ag-1	2.5	2.5	1.0	2.5	41.5
Ag-2	0.25	2.5	1.0	2.5	44.35
Ag-3	2.5	7.5	1.5	10	18.5
Ag-4	2.5	2.5	1.0	5	42.2
Ag-5	2.5	2.5	0.5	2.5	42.0

involves the use of a halogen-containing metal precursor salt (e.g. $HAuCl_4$). The precipitation of AgCl contaminates the alloy nanoparticles formed and further complicates the control of alloy composition.

Herein we report a simple method to prepare Ag–Au alloy nanoparticles by the replacement reaction between Ag nanoparticles and $HAuCl_4$ at elevated temperatures. While this method bears certain similarities with Xia's work [11, 12], the synthesis conditions were altered to deliberately suppress the formation of hollow structures. This method takes advantage of the rapid interdiffusion of Au and Ag atoms in the reduced dimension of nanoparticles, elevated temperature of operation and the large number of interfacial vacancy defects created by the replacement reaction. The major advantages of this method are that both the size and composition of the alloy nanoparticles are independently tunable and that the particles can be produced in high concentrations (good process scalability). This method can also be used to produce other alloy nanoparticles, even those which cannot be obtained by the co-reduction method, e.g. Ag–Pd alloy nanoparticles.

2. Experimental section

Silver nitrate ($AgNO_3$), polyvinylpyrrolidone (PVP, MW = 10 000), potassium hydroxide (KOH) and chlorauric acid ($HAuCl_4{\cdot}3H_2O$) from Aldrich, and sodium borohydride ($NaBH_4$, 98%) from Fluka, were used as received. Deionized water filtered by a Millipore water purification system was the solvent. All glassware and Teflon-coated magnetic stir bars were cleaned in *aqua regia*, followed by copious washing with distilled water before drying in an oven.

PVP-protected Ag nanoparticles were prepared by the $NaBH_4$ reduction of $AgNO_3$. Briefly, 2.5 ml 20 mM $AgNO_3$, 2.5 ml 0.2 M PVP and 1 ml 20 mM KOH were mixed with 41.5 ml H_2O in a sealed 100 ml flask. The solution was stirred under bubbling N_2 for 30 min. 2.5 ml 0.1 M freshly prepared ice-cold $NaBH_4$ solution was then injected into the Ag solution. The mixture was vigorously stirred for 1 h and aged for 48 h to decompose the residual $NaBH_4$. The hydrosol synthesized as such was denoted as Ag-1. A number of other hydrosols containing Ag nanoparticles of varying sizes were obtained by changing the composition of the reaction mixture ($AgNO_3$, PVP, KOH and $NaBH_4$ solution), and were identified as Ag-2, Ag-3 Ag-4 and Ag-5 (table 1).

Ag-1 was used to prepare Ag–Au alloy nanoparticles with different compositions. 20 ml of Ag-1 was refluxed at 100 °C. A measured amount (*vide infra*) of 1 mM $HAuCl_4$ solution was added to the hydrosol under vigorous stirring. The mixture was refluxed for 10 min before it was cooled down to room temperature. The hydrosol was aged for 24 h and then centrifuged at 2000 rpm for 3 min to remove the AgCl precipitate. The supernatant was collected and characterized. The alloy nanoparticles obtained by adding 2.86, 4.44, 5.45 and 6.15 ml of 1 mM of $HAuCl_4$ were labelled as AgAu-1, AgAu-2, AgAu-3 and AgAu-4, respectively. Similarly Ag–Au alloy nanoparticles with the same composition but different sizes were prepared by the replacement reaction between 20 ml of Ag hydrosol (Ag-2, Ag-3, Ag-4 or Ag-5) and 4.44 ml of 1 mM of $HAuCl_4$. The alloy nanoparticles prepared as such were labelled as AgAu-5, AgAu-6, AgAu-7 and AgAu-8, respectively. Ag–Pd alloy nanoparticles with 40 at.% Pd were also prepared by the replacement reaction between 20 ml of Ag-5 and 5.71 ml of 1 mM $PdCl_2$ solution as a demonstration of the general utility of this synthetic approach.

A JEOL JEM2010 field emission transmission electron microscope was used to obtain TEM and HRTEM images and electron diffraction patterns of the nanoparticles. The particle composition was analysed by an EDX analyser attached to the microscope and validated by inductively coupled plasma spectroscopy (ICPS). For TEM measurements a drop of the nanoparticle solution was drop-cast onto a 3 mm copper grid covered with a continuous carbon film. Excess solution was removed with an adsorbent paper and the sample was dried in vacuum at room temperature. UV–visible spectroscopy of the nanoparticle solution was performed on a Shimadzu UV-2450 spectrophotometer.

3. Results and discussion

Since the standard reduction potential of $AuCl_4^-/Au$ (1.0 V versus standard hydrogen electrode, or SHE) is higher than that of the Ag^+/Ag (0.80 V versus SHE), the silver nanoparticles formed upon $NaBH_4$ reduction of Ag^+ were oxidized to Ag^+ by aqueous $HAuCl_4$ solution according to the following replacement reaction:

$$3Ag_{(s)} + AuCl^+_{4(aq)} \rightarrow Au_{(s)} + 3Ag^+ + 4Cl^-_{(aq)}. \qquad (1)$$

The atomic gold produced would then alloy with the unreacted silver under appropriate conditions to form homogeneous alloy nanoparticles. The AgCl by-product was kept in the solution phase by the high temperature of preparation (100 °C) to prevent its deposition on the surface of the alloy nanoparticles. In this way the alloy nanoparticles were free from AgCl contamination[4]. White AgCl precipitate appeared only after the hydrosol was cooled down to room temperature. The AgCl precipitate was crystalline and could be easily removed by

[4] The solubility product of AgCl in water is $\sim 1.8 \times 10^{-10}$ at 20 °C and increases to 1.2×10^{-6} at 100 °C, which is higher than the product of $[Ag^+]$ and $[Cl^-]$ in the preparation.

Table 2. Atomic percentage of Au, absorbance peak and size of nanoparticles.

Nanoparticle	Volume of $HAuCl_4$ solution (ml)	Atomic% of Au	Absorbance (nm)	Average diameter (nm)
Ag-1	0	0	396	8.1
AgAu-1	2.86	19.7	422	7.4
AgAu-2	4.44	40.9	447	6.8
AgAu-3	5.45	61.1	474	6.2
AgAu-4	6.15	80.2	502	5.9

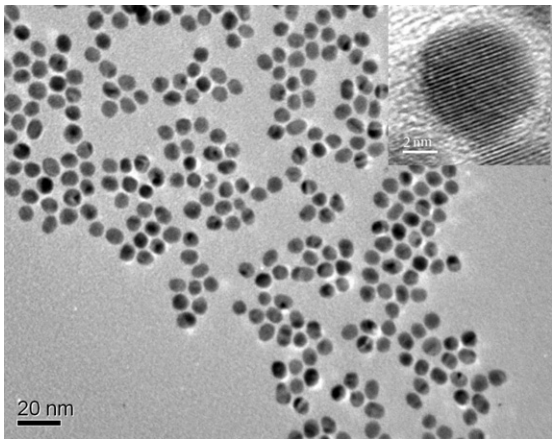

Figure 1. TEM image of Ag nanoparticles. Inset shows the HRTEM image of a Ag nanoparticle.

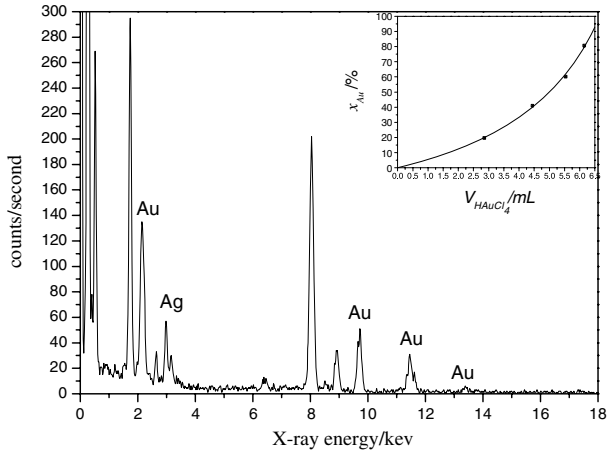

Figure 2. EDX spectrum of alloy nanoparticles from AgAu-2. Inset shows the change of atomic percentage of Au with the volume of 1 mM $HAuCl_4$ solution.

ageing the hydrosol for 24 h or by centrifuging the hydrosol at low speed, e.g. 2000 rpm for 3 min. At this low speed it was impossible to spin down the alloy nanoparticles.

Figure 1 is the TEM image of PVP-protected silver nanoparticles formed upon the $NaBH_4$ reduction of $AgNO_3$. Most particles were nearly spherical with an average diameter of 8.1 nm. The lattice fringes in the HRTEM image (inset of figure 1) are 0.236 nm apart, which agrees well with the (111) lattice spacing of fcc Ag. The colloid was yellowish brown in colour and had an absorbance peak at 396 nm due to SPR.

The compositions of the nanoparticles recovered from the replacement reaction were analysed by EDX and figure 2 shows the EDX spectrum of a typical alloy nanoparticle from AgAu-2. Table 2 provides a summary of the compositions of AgAu-1–4. As one gold atom was formed for every three Ag atoms consumed according to the stoichiometry of the replacement reaction, the at.% of Au in the alloy nanoparticles could be calculated by equation (2):

$$x_{\mathrm{Au}} = \frac{n}{m - 2n} \tag{2}$$

where m and n are the moles of Ag and $HAuCl_4$ used in the preparation. The inset in figure 2 shows good agreement between the experimental measurements and the values calculated from equation (2). In addition to sampling the composition over relatively large areas containing a large number of particles, EDX analysis was also performed on three isolated nanoparticles for each of the colloids. The compositions from these single-particle measurements were very close to the average compositions sampled from collections of particles. Such indication of uniformity in particle-to-particle composition, and the concurrent presence of both Ag and Au in each particle, confirmed that the particles were a Ag–Au alloy and not a physical mixture of monometallic Ag and Au nanoparticles.

Ag and Au nanoparticles and their alloy nanoparticles may be characterized by their absorption in the UV–visible region due to SPR. Figure 3(A) shows the UV–visible spectra of AgAu-1, 2, 3 and 4 together with those of monometallic Ag and Au nanoparticles. The wavelengths at which absorption was maximum are given in table 2. Only one SPR band was detected for each of AgAu-1, 2, 3 and 4 and the absorption maximum was always located between the SPR of monometallic Ag (396 nm) and monometallic Au (523 nm). This is an indication that the nanoparticles were an alloy rather than core–shell nanoparticles, or a mixture of monometallic nanoparticles. It is known that a physical mixture of monometallic Au and Ag nanoparticles has two absorption peaks due to the SPR of Au and Ag, respectively [5]. Core–shell nanoparticles would exhibit the same two absorption peaks, where one increases in absorbance with the increase in the concentration of that component, and a concomitant decrease in the absorbance of the other component [3, 13] However, when the shell becomes thick enough, only the SPR from the shell is detectable [3, 14]. The inset of figure 3(A) shows the absorption peak redshifted linearly and continuously from 396 to 524 nm with the increase in the Au content, which could also be visually detected as a progressive change in the hydrosol colour from light yellow to pink (figure 3(B)). These observations are in agreement with the theoretical predictions in previous papers based on Mie theory [3, 4], further confirming the formation of alloy nanoparticles of homogeneous composition.

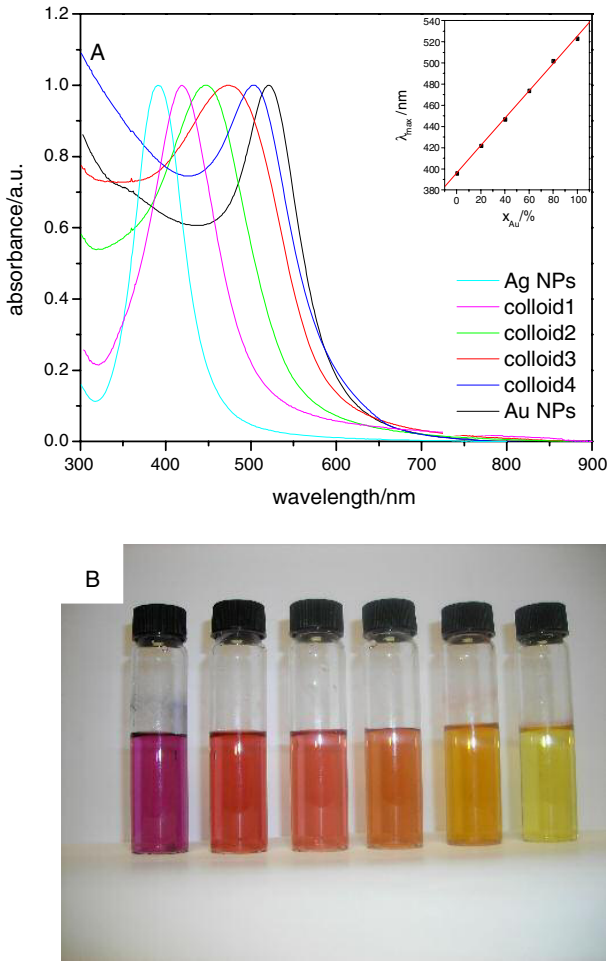

Figure 3. (A) Normalized UV–visible spectra of Ag, Au and alloy nanoparticles. The inset shows the change of absorbance peak with the atomic percentage of Au. (B) Photos of Ag-1, AgAu-1, 2, 3 and 4 and Au nanoparticles (from right to left).

TEM and HRTEM were then used to analyse the bimetallic nanoparticles. TEM images of bimetallic Ag–Au core–shell nanoparticles are known to show banding in electron density with the dark region attributable to gold and the light region attributable to silver [15]. The TEM images of the bimetallic particles prepared here (figure 4) did not show any banding. The uniform contrast for each particle indicates that scattering was distributed evenly throughout the particle volume, which is only possible if the particles were alloy. The absence of electron density banding was also confirmed by HRTEM. Figure 5 shows the HRTEM image of the nanoparticle in AgAu-2. The nanoparticles in AgAu-1, 3 and 4 had a similar appearance except for the size of the particles. Figure 5 shows excellent atomic ordering within each particle. There was no lattice mismatch as expected from the highly similar lattice constants of 0.408 for Au and 0.409 for Ag. The experimentally observed uniform contrast throughout the particle volume was another demonstration of good atomic level mixing.

Figure 6 shows the electron diffraction pattern of particles sampled from AgAu-2. The radii of the four ring patterns are in ratios of $\sqrt{3}$:$\sqrt{4}$:$\sqrt{8}$:$\sqrt{11}$, corresponding to the 111, 200, 220 and 311 reflection of the fcc structure and hence confirm the alloy nanoparticles to be isostructural with the starting Ag nanoparticles. The electron diffraction pattern is also indistinguishable from those of monometallic silver and gold nanoparticles because the Ag–Au alloy adopted the fcc structure of Ag and Au which have closely matched lattice constants. The electron diffraction patterns of other alloy nanoparticles are similar to this one.

TEM images also showed a contraction in the starting Ag nanoparticle diameter after the replacement reaction (figure 4). Indeed there was a systematic decrease in the diameter of the alloy nanoparticles with the increase in Au content. This is to be expected from the stoichiometry of the replacement reaction which requires three silver atoms to be consumed for every gold atom deposited. There was therefore a net reduction in the total number of atoms per particle. Since the Au–Ag alloy has an identical crystal structure to Ag and the size of Au and Ag atoms are similar, the dependence of particle diameter on the number of atoms in a particle could be approximated by equation (3):[5]

$$\frac{d_{\text{alloy}}}{d_{\text{Ag}}} = \sqrt[3]{\frac{m-2n}{m}}. \tag{3}$$

Figure 7 shows that the experiment results are in reasonably good agreement with the values calculated from this simple relationship.

Ag–Au alloy nanoparticles with the same composition (40% of Au) but variable sizes were also prepared. The TEM images (figure 8) of these nanoparticles show average diameters of 2.8, 4.6, 6.2 and 9.1 nm. According to equation (3), the size of alloy nanoparticles of the same composition is dependent on the size of the Ag nanoparticle seeds, which can be easily tuned by changing the synthesis conditions such as the concentrations of Ag^+ and the protective agent, pH and ratio between Ag^+, $NaBH_4$ and PVP (table 1)

It is an interesting observation that homogeneous alloy nanoparticles were formed as a result of the replacement reaction. This indicates that the alloying between Au and Ag was concurrent with the replacement reaction. It is known that a homogeneous solid solution of Ag and Au is thermodynamically more stable than pure Au or Ag [16]. Alloy formation requires the interdiffusion of Au and Ag atoms, which is generally slow for bulk gold and silver. However, the rate of diffusion can increase rapidly with the decrease in particle dimension, increase in temperature and the presence of vacancy defects [17–21]. The increase in interdiffusion rate

[5] Since the Au–Ag alloy was structurally similar to Ag, and Ag and Au atoms have approximately the same size, the volume of a particle (V) is approximately proportional to the number of atoms in the particle (N). The number of atoms in the starting Ag nanoparticles, N_{Ag}, is proportional to the moles of Ag precursor present (m). The displacement reaction replaced 3 Ag atoms by 1 Au atom, and the number of atoms that remained after reacting m moles of Ag^+ with n moles of $HAuCl_4$ would be $(m-3n)+n = m-2n$. i.e.

$$\frac{V_{\text{alloy}}}{V_{\text{Ag}}} = \frac{N_{\text{alloy}}}{N_{\text{Ag}}} = \frac{m-2n}{m}.$$

The ratio of diameters could then be approximated by the cube root of the volume ratio, assuming spherical geometry, i.e.

$$\frac{d_{\text{alloy}}}{d_{\text{Ag}}} = \sqrt[3]{\frac{V_{\text{alloy}}}{V_{\text{Ag}}}} = \sqrt[3]{\frac{m-2n}{m}}.$$

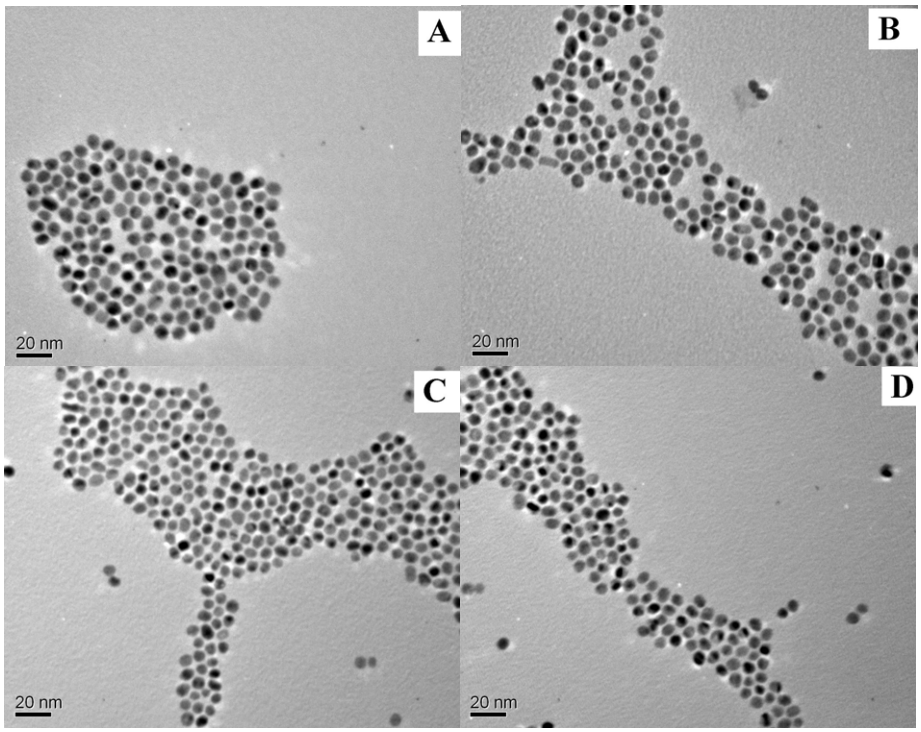

Figure 4. (A)–(D): TEM images of nanoparticles from AgAu-1, 2, 3 and 4.

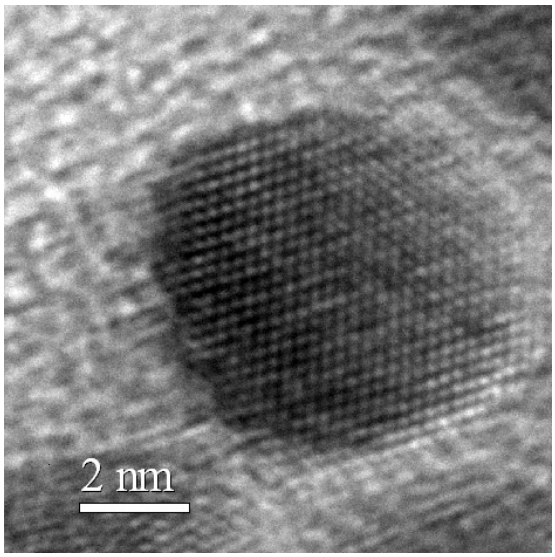

Figure 5. HRTEM image of a nanoparticle in AgAu-2.

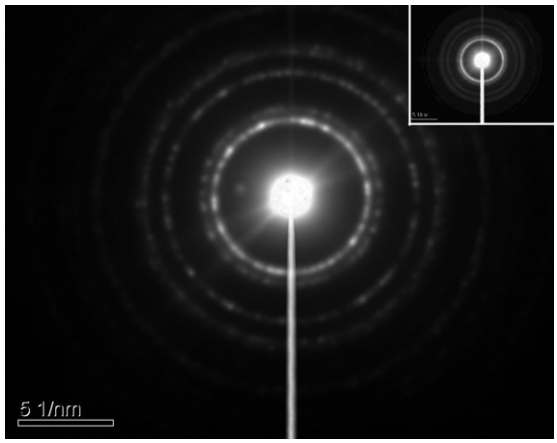

Figure 6. Electron diffraction (ED) pattern of nanoparticles from AgAu-2. The inset shows the diffraction pattern from Ag nanoparticles. The four rings (from inner to outer) correspond to the 111, 200, 220 and 300 reflections.

by reduced dimension has been witnessed before: the magnitude of interdiffusion coefficient of Ag and Au was found to be strongly particle-size-dependent [17]. Dick and coworkers [18] measured the diffusion coefficient of gold in 2 nm gold nanoparticles to be about 10^{-24} cm^2 s^{-1} at room temperature, orders of magnitude higher than the value of 10^{-32} cm^2 s^{-1} for bulk gold. Rapid interdiffusion of metal atoms on the nanometre scale has also been experimentally confirmed by the rapid alloying of two metals when one of them was deposited on the nanoparticles of the other even at ambient temperature [19]. The interdiffusion of gold and silver atoms also benefits greatly from the increase in temperature [20]. According to the Arrhenius equation, the interdiffusion coefficient increases from 10^{-24} to 10^{-19} cm^2 s^{-1} when the temperature is increased from 20 to 100 °C [10]. Furthermore, vacancy defects at the interface between the two metals also contribute to the interdiffusion rate [21]. A large number of vacancies were created during the replacement reaction since three silver atoms had to be removed for every gold atom deposited. The use of small Ag nanoparticle templates and elevated temperatures, and the presence of a large number of

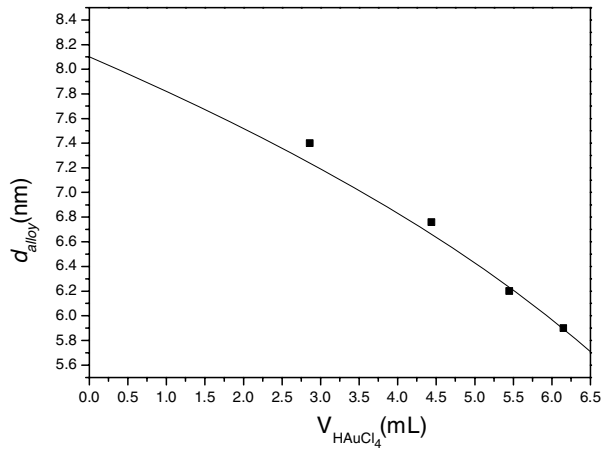

Figure 7. The change of alloy nanoparticle size with the volume of 1 mM $HAuCl_4$ solution.

vacancy defects created by the replacement reaction in the current method of preparation, fulfil the conditions for rapid alloy formation, and the ease of formation of homogeneous alloy nanoparticles is not totally unexpected.

This current method of preparation has some very notable advantages: (1) ease of control of both the size and composition of the alloy nanoparticles; (2) the alloy nanoparticles can be produced in high concentrations; (3) it can be used to prepare alloy nanoparticles that cannot be obtained by the co-reduction method.

One major advantage of the current method is the ease of tuning the size and composition of the alloy nanoparticles. The size of nanoparticles is often tuned by controlling the environmental factors in the nucleation and growth process (e.g. nature of the reducing and stabilizing agents, precursor concentration, ratios of reducing and stabilizing agents to the precursor, and temperature). Tuning the size of alloy nanoparticles is a great challenge while it is relatively easy for the monometallic nanoparticles. This is because the composition of alloy nanoparticles is also strongly dependent on the environmental factors and changes in the latter can bring about simultaneous changes in both size and composition. The current method of preparation offers independent size and composition control, thereby decoupling the environmental impact on these two important product attributes. The composition of the alloy nanoparticles is controlled by the $HAuCl_4$ to Ag ratio according to equation (2). With m and n specified the size of the alloy nanoparticles is controlled by the size of the Ag nanoparticles (d_{Ag}) according to equation (3). In addition, the size of the monometallic Ag nanoparticle seeds can be varied in a number of ways according to established procedures [22]. As the properties of alloy nanoparticles depend on both size and composition, the ability for individual tuning of size and composition can significantly increase the degrees of freedom in tailoring the properties of the alloy nanoparticles for enhanced application performance.

The second major advantage of the current method is the production of alloy nanoparticles in relatively high concentrations. In the commonly used co-reduction method, the alloy nanoparticles have to be produced in very low concentrations (less than 10^{-5} M) to prevent the contamination of the product nanoparticles by AgCl because of the low solubility product of the latter in water at 20 °C ($k_{sp} = \sim 1.8 \times 10^{-10}$). The solubility product of AgCl is increased by four

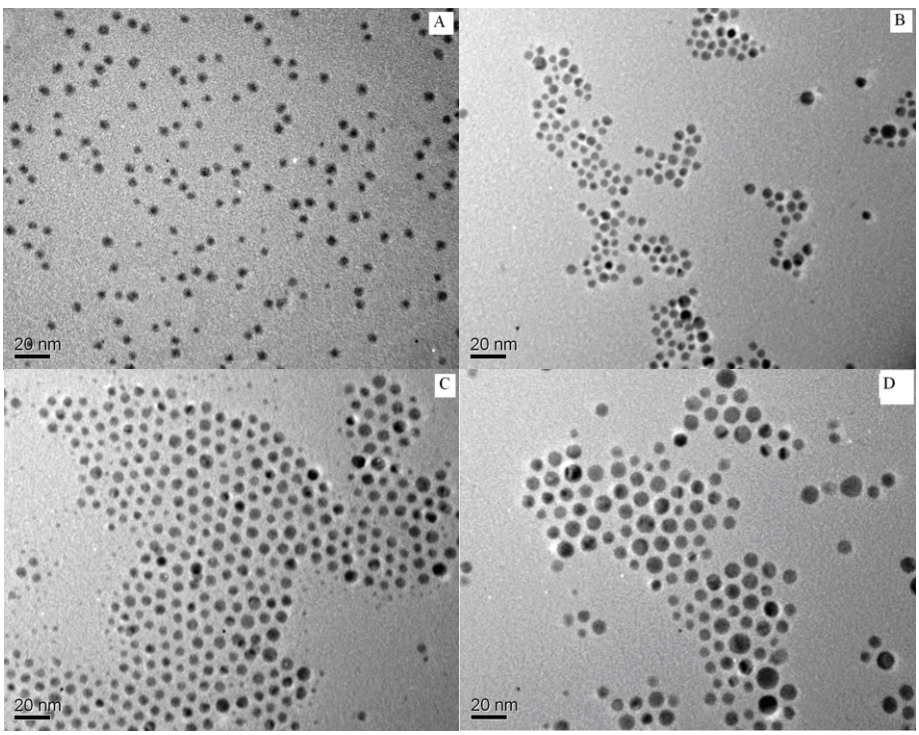

Figure 8. TEM images of 40% Au alloy nanoparticles with different size. (A) 2.8 nm(AgAu-5), (B) 4.6 nm(AgAu-6), (C) 6.2 nm(AgAu-7), (D) 9.1 nm(AgAu-8).

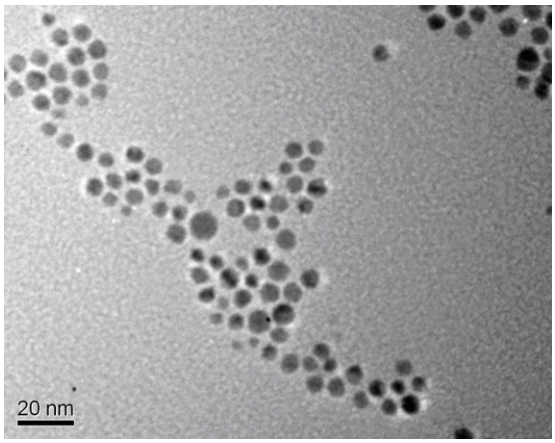

Figure 9. TEM image of Ag–Pd alloy nanoparticles.

times at 100 °C; correspondingly the usable Ag^+ concentration is about two orders of magnitude higher than what is possible with co-reduction at room temperature. Therefore in the replacement reaction carried out at 100 °C, the silver chloride formed was completely soluble. The Ag^+ concentration in the solution could be 10^{-3} M or higher, depending on the composition of the alloy. Solid AgCl was salted out from the solution only after the hydrosol was cooled down to room temperature, and it could be easily removed as a separate phase while the alloy particles stayed suspended in the solution. The ability to use temperature manipulation to separate the two products of the replacement reaction allows the alloy nanoparticles to be produced in relatively pure form without AgCl contamination and in high concentrations. Compared with the preparation of alloy nanoparticles by co-reduction at 100 °C carried out by Link [4], the alloy nanoparticles produced by the replacement reaction at 100 °C were much smaller, with improved ease of independent size and composition control.

Another advantage of the current method is that it can produce nanoparticles that cannot be prepared by the co-reduction method. A good example is the Ag–Pd system where co-reduction of Ag and Pd precursors would only produce core–shell nanoparticles instead of alloy nanoparticles due to the difference in the reduction potentials of Ag and Pd. On the other hand Ag–Pd alloy nanoparticles can be prepared relatively easily by the current method (figure 9). The preparative protocol is extendable to any alloy system provided the following requirements are met: (1) reducibility of the precursor of one metal by the nanoparticles of the other metal; and (2) the two metals must have the same crystal structure and similar lattice parameters to enable complete solid solution formation. These conditions are also met by the Ag–Pd system, namely the oxidizability of Ag nanoparticle by Pd^{2+} ($E(Pd^{2+}/Pd) = 0.95$ V (SHE), $E(Ag^+/Ag) = 0.80$ V SHE)) and the likeness of Ag and Pd in crystal structure (fcc) and lattice parameter.

Our results did not contradict those of other authors despite their apparent differences since the replacement reaction was carried out under different conditions. The replacement reaction between Ag nanoparticles and $HAuCl_4$ involves a number of steps including the oxidative dissolution of Ag atoms, the reduction of $AuCl_4^-$ and deposition of the Au atoms formed, and the counterdiffusion of vacancies and atoms. Usually, Ag dissolution and Au deposition occur on different sites, thereby allowing the Au atoms to alloy with the unreacted Ag atoms. The rates of Ag dissolution, Au atom deposition and the interdiffusion of Ag and Au atoms and vacancies are dependent on the crystal structure of the Ag nanoparticles (for example, single-crystal cubooctahedral, multiply twinned decahedral or icosahedral) and environmental factors such as temperature, solvent and the effectiveness of the stabilizing agent. The vacancy defects created in the replacement reaction are annihilated by forming an internal cavity or by diffusion to the outer surface of the particle. In the case of small nanoparticles (<10 nm in the current case), the enhanced diffusion rate due to reduced particle dimension and the small thickness ease the diffusion of vacancy defects to the outer surface. Even in the event that small voids are present inside a particle, Ostwald ripening will occur quickly to transform the particle into a solid one to lower its total surface energy. Consequently solid nanoparticles were formed as the primary product.

4. Conclusion

Au–Ag alloy nanoparticles were prepared by the replacement reaction between Ag nanoparticles and $HAuCl_4$ at 100 °C. UV–visible spectroscopy, SAEDX, TEM and HRTEM all confirmed the formation of homogeneous alloy nanoparticles. The alloy nanoparticles were formed by the rapid interdiffusion of Au and Ag atoms as a result of the reduced dimension of the silver nanoparticles, elevated temperature and the large number of interfacial vacancy defects generated by the replacement reaction. The method has several notable advantages such as the ease of independent control of both size and composition of the alloy nanoparticles, and the production of the alloy nanoparticles in relatively high concentrations. This method can also be used to prepare alloy nanoparticles which cannot be obtained by the common co-reduction method, such as Ag–Pd.

Acknowledgments

The authors thank Mr P A Chai and Mr Z Shang for their helpful suggestions on TEM measurements.

References

[1] Sun S H, Murray C B, Weller D, Folks L and Moser A 2000 *Science* **287** 1989
Toshima N, Harada M, Yamazaki Y and Asakura K 1992 *J. Phys. Chem.* **96** 9927
[2] Liu J H, Wang A Q, Chi Y S, Lin H P and Mou C Y 2005 *J. Phys. Chem.* B **109** 40
Wang A Q, Liu J H, Lin S D, Lin T S and Mou C Y 2005 *J. Catal.* **233** 186
[3] Mulvaney P 1996 *Langmuir* **12** 788
[4] Link S, Wang Z L and El-Sayed M A 1999 *J. Phys. Chem.* B **103** 3529
[5] Mallin M P and Murphy C J 2002 *Nano Lett.* **2** 1235
[6] Wilson O M, Scott R W J, Garcia-Martinez J C and Crooks R M 2005 *J. Am. Chem. Soc.* **127** 1015

Senapati S, Ahmad A, Khan M I, Sastry M and Kumar R 2005 *Small* **1** 517
Hostetler M J *et al* 1998 *J. Am. Chem. Soc.* **120** 9396
Kariuki N N *et al* 2004 *Langmuir* **20** 11240
[7] Chen D H and Chen C J 2002 *J. Mater. Chem.* **12** 1557
[8] Smetana A B, Klabunde K J, Sorensen C M, Ponce A A and Mwale B 2006 *J. Phys. Chem.* B **110** 2155
[9] Chen Y H and Yeh C S 2001 *Chem. Commun.* 371
Lee I, Han S W and Kim K 2001 *Chem. Commun.* 1782
Izgaliev A T, Simakin A V and Shafeev G A 2004 *Quantum Electron.* **34** 47
[10] Papavassiliou G C 1976 *J. Phys. F: Met. Phys.* **6** L103
[11] Sun Y G, Mayers B T and Xia Y N 2002 *Nano Lett.* **2** 481
Liang H P, Wan L J, Bai C L and Jiang L 2005 *J. Phys. Chem.* B **109** 7795
Selvakannan P R and Sastry M 2005 *Chem. Commun.* (Issue 13) 1684
[12] Sun Y G and Xia Y N 2004 *J. Am. Chem. Soc.* **126** 3892
[13] Mallik K, Mandal M, Pradhan N and Pal T 2001 *Nano Lett.* **1** 319
[14] Lu L H, Wang H S, Zhou Y H, Xi S Q, Zhang H J, Jiawen H B W and Zhao B 2002 *Chem. Commun.* (Issue 14) 144
[15] Srnova-Sloufova I, Lednicky F, Gemperle A and Gemperlova J 2000 *Langmuir* **16** 9928
[16] Shi H Z, Zhang L D and Cai W P 2000 *J. Appl. Phys.* **87** 1572
[17] Ouyang G, Tan X, Wang C X and Yang G W 2006 *Chem. Phys. Lett.* **420,** 65
[18] Dick K, Dhanasekaran T, Zhang Z Y and Meisel D 2002 *J. Am. Chem. Soc.* **124** 2312
[19] Yasuda H and Mori H 1992 *Phys. Rev. Lett.* **69** 3747
Yasuda H, Mori H, Komatsu M and Takeda K 1993 *J. Appl. Phys.* **73** 1100
[20] Wonnell S K, Delaye J M, Bibole M and Limoge Y 1992 *J. Appl. Phys.* **72** 5195
Ding Y and Erlebacher J 2003 *J. Am. Chem. Soc.* **125** 7772
[21] Shibata T, Bunker B A, Zhang Z Y, Meisel D, Vardeman C F and Gezelter J D 2002 *J. Am. Chem. Soc.* **124** 11989
[22] Pavlyukhina L A, Zaikova T O, Odegova G V, Savintseva S A and Boldyrev V V 1998 *Inorg. Mater.* **34** 109
He B L, Tan J J, Kong Y L and Liu H F 2004 *J. Mol. Catal.* A **221** 121
Murthy S, Bigioni T P, Wang Z L, Khoury J T and Whetten R L 1997 *Mater. Lett.* **30** 321